

**INTRODUCTION:** 60018 is a coherent, medium gray, basaltic impact melt that suffered a variety of shock effects after lithification. Extensive fractures and a network of glass veins penetrate the rock (Fig. 1). A dark, vesicular glass coats the exterior surfaces.

60018 was chipped from a 50 cm boulder 100 m southwest of the Lunar Module. This boulder was perched and subrounded. The location and orientation of 60018 are known. Many zap pits are present on the lunar-exposed surface.



FIGURE 1. Saw-cut face. S-78-31788.

**PETROLOGY:** Although intensely shocked, a relict melt texture is clearly discernable over much of the rock. An intergranular basaltic texture is most common with plagioclase laths often forming radial clusters (Fig. 2). Areas of fine-grained breccia and patches with a poikilitic to subophitic texture are also present. Grain size of the melt matrix varies dramatically over short distances; maximum crystal length is ~1 mm.

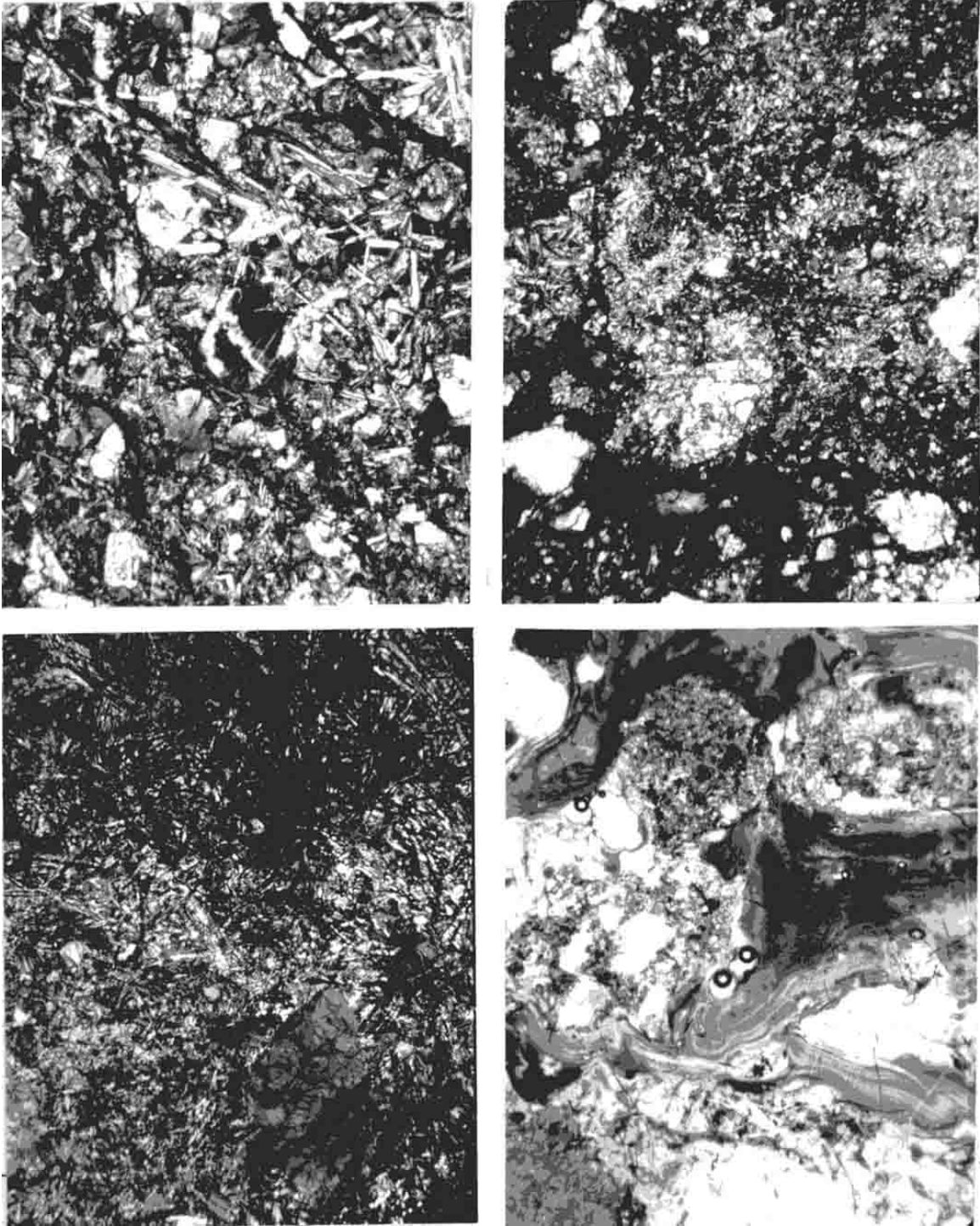


FIGURE 2.

- a) 60018,53. general view, basaltic, xpl. width 2 mm.
- b) 60018,57. general view, poikilitic and glassy, xpl. width 2 mm.
- c) 60018,51. spherulitic, glassy, xpl. width 2mm.
- d) 60018,51. glass veins, ppl. width 2 mm.

Plagioclase xenocrysts are abundant. Clasts of anorthosite and noritic anorthosite (up to ~1 cm) are somewhat less common. Metal fragments have Ni and Co contents which plot within the “meteoritic field” (Reed and Taylor, 1974). Troilite and schreibersite are occasionally associated with the metal. Figure 3 shows that many of the kamacite particles not associated with schreibersite are nevertheless enriched in P relative to meteoritic metal. Some rust is also present. Late stage silicate-liquid immiscibility is apparent in some interstitial areas.

Both the clasts and the host basalt show extreme shock effects. Many of the plagioclase laths and clasts have been converted to maskelynite or recrystallized. In the most severely altered zones interstitial mafics have been converted to small rounded grains (Fig. 2).

A complex network of glass veins penetrates the rock and is probably related to the glass coat. In thin section these veins are green to brown, often contain schlieren and debris, and seem especially common along clast-matrix boundaries. The intrusion of these glass veins appears to postdate the lithification of the rock and is probably related to the event which caused the intense shock metamorphism.

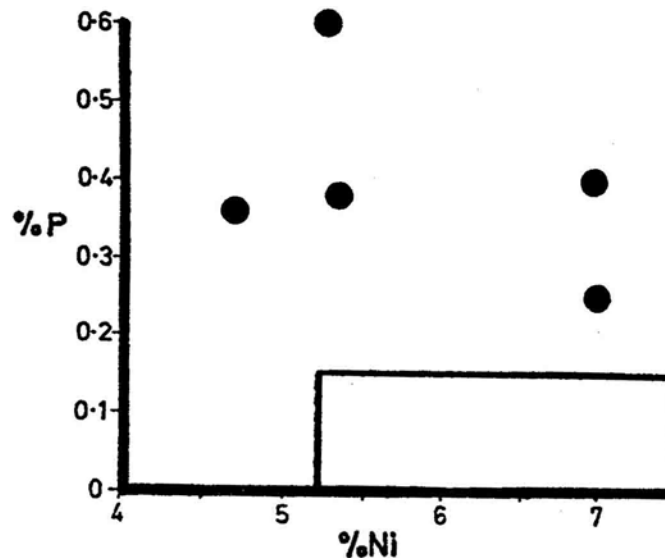


FIGURE 3. P vs. Ni for metal; from Reed and Taylor (1974).

CHEMISTRY: S.R. Taylor et al. (1973) and Haskin (unpublished) have analyzed bulk rock samples for major and trace elements. Haskin (unpublished) has also analyzed clasts and glass samples. Cripe and Moore (1974), Moore and Lewis (1976), Moore et al. (1973) and Goel et al. (1975) provide carbon, nitrogen and sulfur data. Nunes et al. (1974) provide U, Th, and Pb abundances.

REEs in the basalt are high (Fig. 4). This, along with the high bulk Ni values and metal composition indicates that the rock was a clast-laden impact melt with significant KREEP and meteoritic components. Also notable is the extreme enrichment in sulfur relative to the other light elements (Table 1).

The glass veins are significantly more aluminous than the basalt and have lower levels of incompatible elements (Table 1). Thus the glass is not a whole rock melt of the basalt.

White clasts analyzed by Haskin are virtually pure plagioclase or anorthosite based on their low contents of FeO and REEs (Table 1). One black clast, also analyzed by Haskin, is ultramafic with high FeO and very low levels of REEs (Table 1).

TABLE 1. Summary chemistry of the melt matrix (basalt), clasts and glass veins of 60018.

	<u>Basalt</u>	<u>Glass *</u>	<u>White clasts *</u>	<u>Black clasts *</u>
SiO <sub>2</sub>	45.7	44.9		
TiO <sub>2</sub>	0.65	0.359		
Al <sub>2</sub> O <sub>3</sub>	24.0	28.5		
Cr <sub>2</sub> O <sub>3</sub>	0.11	0.086	0.006	0.04
FeO	5.6	4.60	0.3	34.8
MnO	0.07	0.048	0.015	1.07
MgO	8.9	4.83		
CaO	13.8	16.6		
Na <sub>2</sub> O	0.54	0.492	0.424	0.02
K <sub>2</sub> O	0.23	0.103		
P <sub>2</sub> O <sub>5</sub>				
Sr				
La	25	10.7	0.38	(Sm=0.042)
Lu	1.1	0.46	0.003	
Rb	7.7	3.1		
Sc	9.1	6.0	0.44	7.1
Ni	400	520		
Co	29	43	0.54	71
Ir ppb				
Au ppb				
C	32			
N	29			
S	2250			
Zn	2.2	2.6		
Cu				

Oxides in wt%; others in ppm except as noted.

\*from Haskin (unpublished)

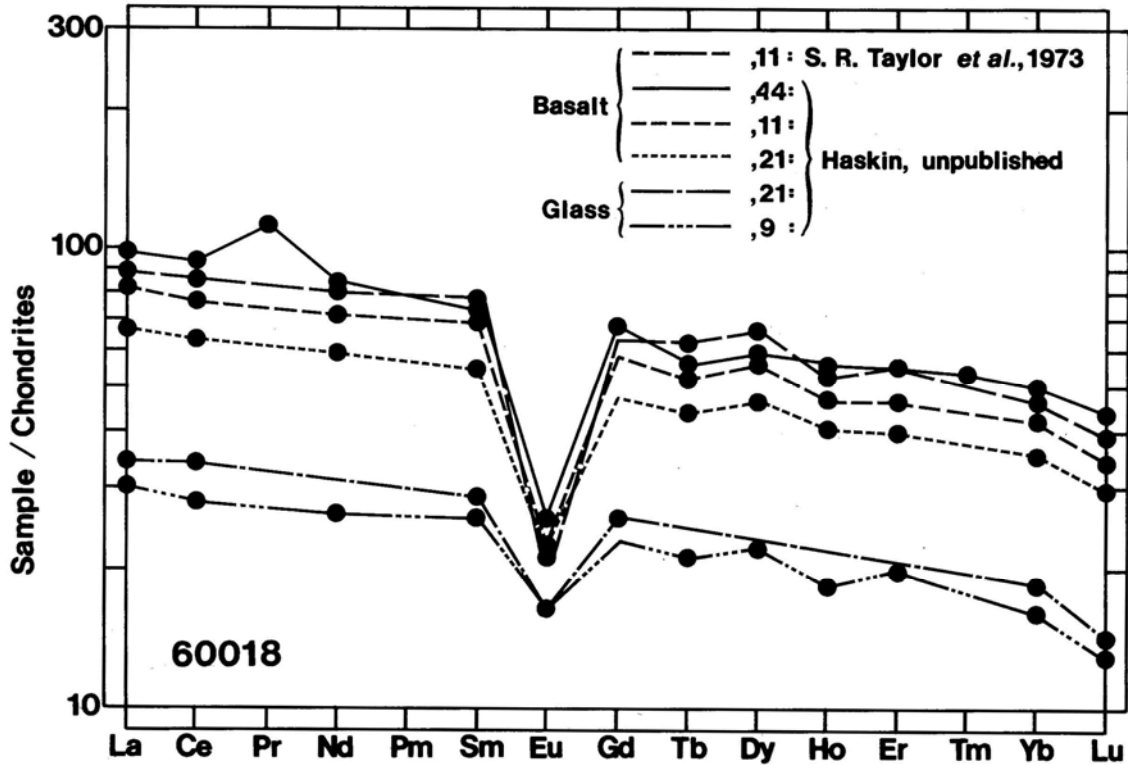


FIGURE 4. Rare earths.

TABLE 2. Oxygen isotope data.

	$\delta O^{18}$	$\delta O^{17}$
Whole rock	5.69	
Light clast	5.60	
"Cataclastic anorthosite"*	5.60	2.75

\*Listed in Clayton and Mayeda (1975) as 60018,43.  
 Photodocumentation shows that this split is mostly basalt but also contains a large white clast.

STABLE ISOTOPES: Clayton et al. (1973) and Clayton and Mayeda (1975) report  $\delta O^{18}$  and  $\delta O^{17}$  data for clasts and the bulk rock (Table 2).

RADIOGENIC ISOTOPES AND GEOCHRONOLOGY: Nunes et al. (1974, 1977) provide U-Th-Pb data for several splits of the rock. Many of their samples had sawn surfaces and were significantly (up to 77%) contaminated with terrestrial lead (Fig. 5). Only their "whole rock" and hand-picked glass samples do not appear to be

contaminated. The “whole rock” analysis is nearly concordant at 4.2 b.y. but the glass contains excess Pb relative to U suggesting that the glass may be fused soil (Nunes et al., 1974,1977).

**PHYSICAL PROPERTIES:** Sugiura et al.(1978) report the results of paleointensity experiments performed while heating the sample under controlled  $fO_2$  (Thellier’s method) (Fig. 6). The natural remanent magnetization (NRM) of the rock is fairly strong and stable against AF-demagnetization although an ancient remanent magnetization probably is not present. As most of the NRM is thermally demagnetized by  $400^\circ\text{C}$ , low temperature shock events may have been responsible for the remanent magnetization that is present. Some of the magnetic properties can also be accounted for by the chemical changes produced by heating.

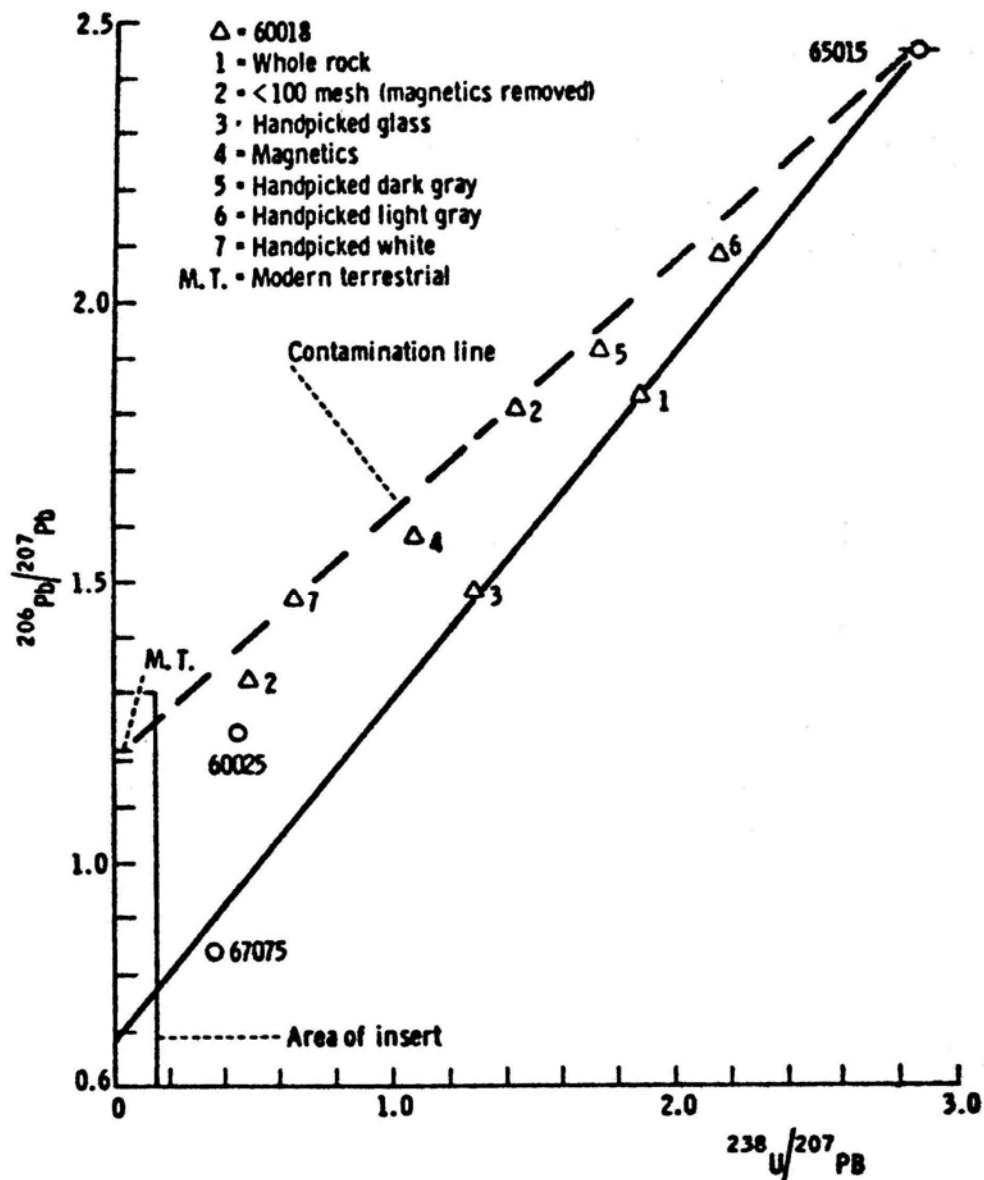
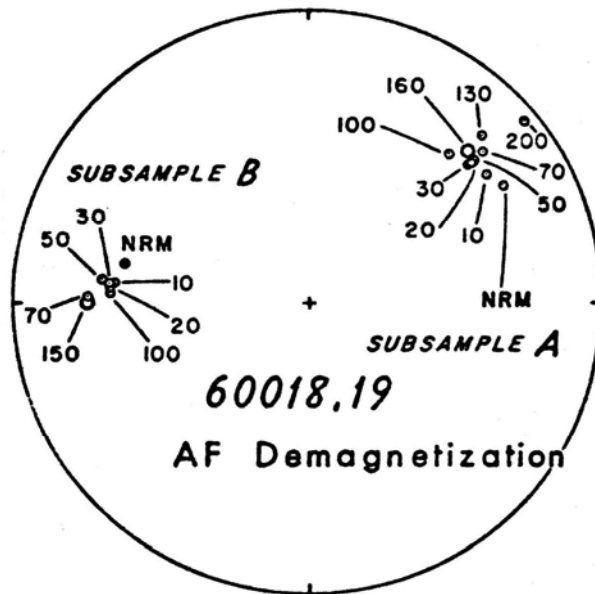
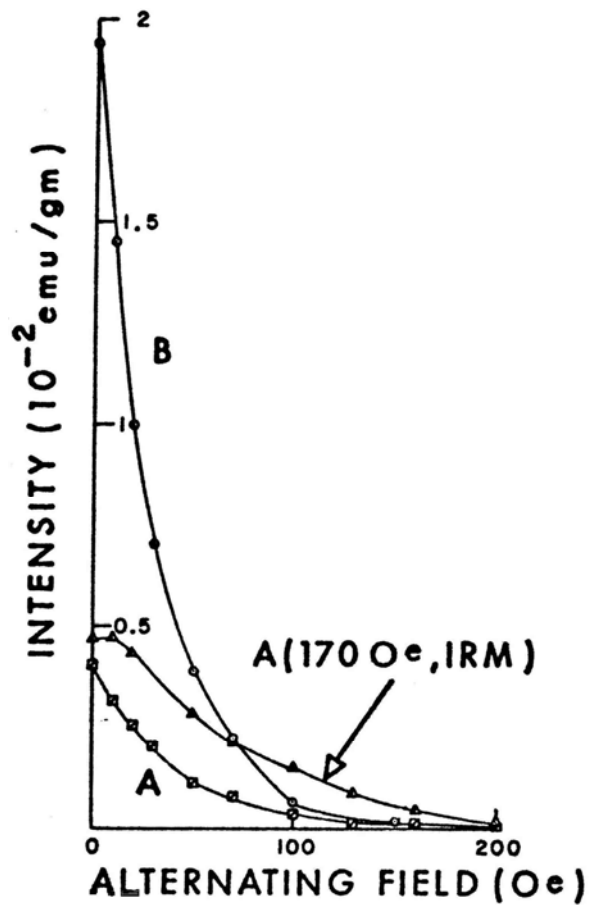


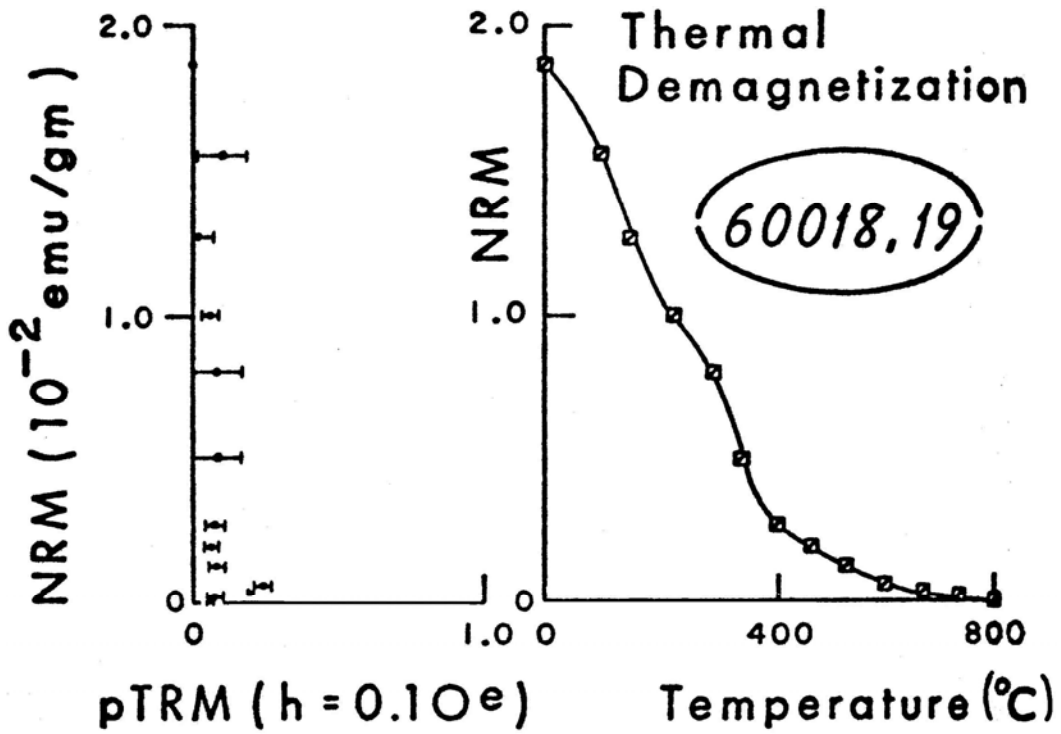
FIGURE 5. U-Pb data; from Nunes et al. (1977).



Directional change of NRM during AF demagnetization for two pieces of 60018,19. Relative orientation of these two pieces is not known.



AF demagnetization of NRM for two pieces (A and B) of 60018,19 and of IRM for piece A.



NRM vs. pTRM plot and thermal demagnetization for 60018,19.

FIGURE 6. Demagnetization; from Sugiura et al. (1978).

PROCESSING AND SUBDIVISIONS: In 1972 this rock was cut into three main pieces, one being a slab (Fig. 7). The slab was entirely subdivided with most of the allocations being taken from it. Not all splits are shown in the diagram.

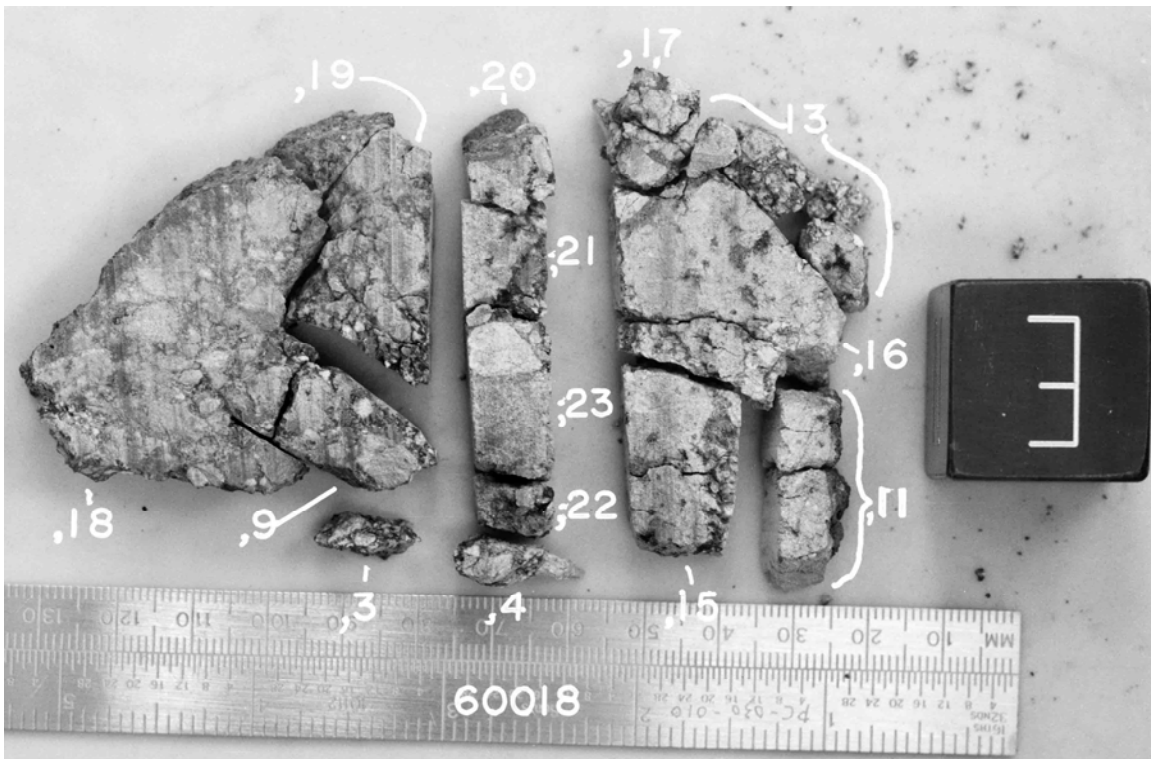
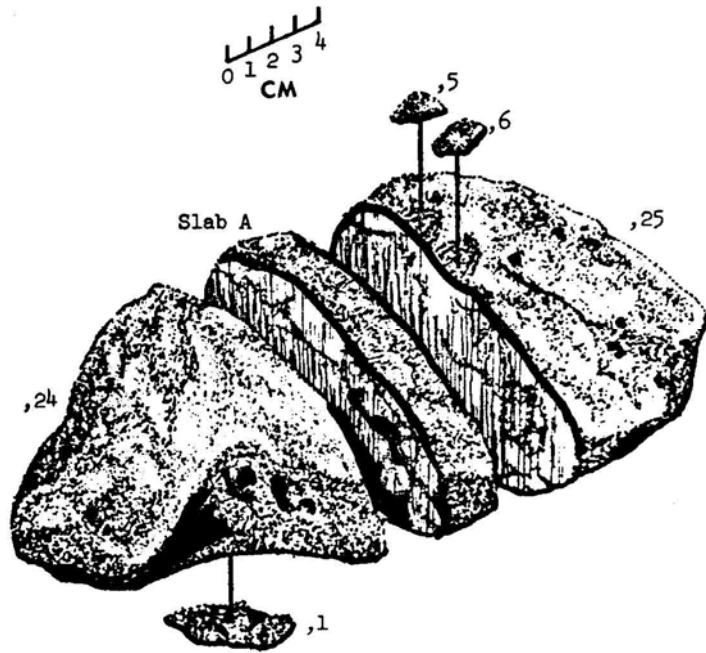


FIGURE 7. Top: cutting diagram. Bottom: slab dissection. S-73-21540.